BIOCHEMISTRY

Lytic polysaccharide monooxygenase increases cellobiohydrolases activity by promoting decrystallization of cellulose surface

Taku Uchiyama[1], Takayuki Uchihashi[2,3], Takuya Ishida[1]†, Akihiko Nakamura[4], Josh V. Vermaas[5,6], Michael F. Crowley[5], Masahiro Samejima[1,7], Gregg T. Beckham[5], Kiyohiko Igarashi[1,8]*

Efficient depolymerization of crystalline cellulose requires cooperation between multiple cellulolytic enzymes. Through biochemical approaches, molecular dynamics (MD) simulation, and single-molecule observations using high-speed atomic force microscopy (HS-AFM), we quantify and track synergistic activity for cellobiohydrolases (CBHs) with a lytic polysaccharide monooxygenase (LPMO) from *Phanerochaete chrysosporium*. Increasing concentrations of LPMO (AA9D) increased the activity of a glycoside hydrolase family 6 CBH, Cel6A, whereas the activity of a family 7 CBH (Cel7D) was enhanced only at lower concentrations of AA9D. MD simulation suggests that the result of AA9D action to produce chain breaks in crystalline cellulose can oxidatively disturb the crystalline surface by disrupting hydrogen bonds. HS-AFM observations showed that AA9D increased the number of Cel7D molecules moving on the substrate surface and increased the processivity of Cel7D, thereby increasing the depolymerization performance, suggesting that AA9D not only generates chain ends but also amorphizes the crystalline surface, thereby increasing the activity of CBHs.

INTRODUCTION

Cellulosic biomass is a potential feedstock for sustainable energy and bio-based material production, and therefore, basic studies of its enzymatic deconstruction are important for bio-based carbon cycling. Because cellulose is an insoluble crystalline substrate and is highly recalcitrant to depolymerization, synergistic deconstruction by cellulolytic enzymes performing various functions plays a key role. Cellulases—namely, cellulolytic glycoside hydrolases (GHs)—can be categorized into cellobiohydrolases (CBHs), endoglucanases (EGs), and β-glucosidases (*1*). Among them, CBHs depolymerize crystalline cellulose by processive hydrolysis along a cellulose chain, where successive hydrolysis events can occur without enzyme dissociation from the chain. EGs hydrolyze cellulose chains in amorphous regions at internal sites of a cellulose chain, and β-glucosidases hydrolyze cello-oligosaccharides produced by CBH and/or EG activities, relieving product inhibition.

Beyond GHs, lytic polysaccharide monooxygenases (LPMOs) were discovered as a group of oxidative cellulolytic enzymes (*2*, *3*). LPMOs form a redox couple that catalyzes oxidative cleavage of glycosidic bonds and are the main enzymes involved in oxidative boosting of crystalline cellulose degradation. The LPMO-mediated reaction requires electrons, which can be provided by external reducing agents (*4*–*7*), enzymatic systems such as cellobiose dehydrogenase (CDH) (*8*–*10*), or a photocatalytic system (*11*). Recent studies have suggested that H_2O_2 is a cosubstrate of LPMOs (*12*). LPMO activity enhances the activity of glycosyl hydrolytic enzymes toward highly crystalline substrates that are resistant to cellulases (*13*–*17*) and increases the activity of cellulosic enzyme cocktails (*18*–*20*). However, some combinations of LPMO and cellulase do not show such synergy (*14*, *16*, *17*), suggesting that further study of the synergy mechanisms between LPMO and GHs merits attention.

The white-rot fungus *Phanerochaete chrysosporium* degrades all plant cell wall components and is among the best-studied fungi associated with woody biomass bioconversion (*21*). *P. chrysosporium* produces many types of extracellular GHs and oxidative enzymes (*22*), and the molecular structures of two CBHs, Cel6A and Cel7D, have been solved (*23*, *24*). Furthermore, processive movements of Cel7D have been visualized by high-speed atomic force microscopy (HS-AFM) (*25*). As shown in Fig. 1A, the molecular structure of the *P. chrysosporium* LPMO, AA9D, has also been solved (*26*), and its biochemical characteristics, strict C-1 hydroxyl group oxidation specificity, and inability to degrade cello-oligosaccharides were also reported (*27*).

In the present work, we chose these well-characterized enzymes to analyze how AA9D affects the hydrolytic activity of CBHs by following the time course for hydrolytic product formation from highly crystalline cellulose I_α from green algae, *Cladophora* spp. (*28*). We also used molecular dynamics (MD) simulations to evaluate the effect of AA9D activity on the crystalline cellulose surface and HS-AFM to observe crystalline cellulose degradation by Cel7D and AA9D at the molecular level.

[1]Department of Biomaterial Sciences, Graduate School of Agricultural and Life Sciences, The University of Tokyo, 1-1-1 Yayoi, Bunkyo-ku, Tokyo 113-8657, Japan. [2]Department of Physics and Structural Biology Research Center, Nagoya University, Chikusa-ku, Nagoya, 464-8602, Japan. [3]Department of Physics, Structural Biology Center, and Institute for Glyco-core Research (iGCORE), Nagoya University, Nagoya, 464-8602, Japan. [4]Department of Applied Life Sciences, Faculty of Agriculture, Shizuoka University, Suruga-ku, Shizuoka 422-8529, Japan. [5]Renewable Resources and Enabling Sciences Center, National Renewable Energy Laboratory, Golden, CO 80401, USA. [6]MSU-DOE Plant Research Laboratory and Department of Biochemistry and Molecular Biology, Michigan State University, East Lansing, MI 48824, USA. [7]Faculty of Engineering, Shinshu University, 4-17-1, Wakasato, Nagano 380-8533, Japan. [8]VTT Technical Research Center of Finland Ltd., Tietotie 2, P.O. Box 1000, Espoo, FI-02044 VTT, Finland.
†Present address: IMEQRD Co. Ltd., Daiwa Ginza Bldg. 3F, 6-2-1 Ginza, Chuo-ku, Tokyo 104-0061, Japan.
*Corresponding author. Email: aquarius@mail.ecc.u-tokyo.ac.jp

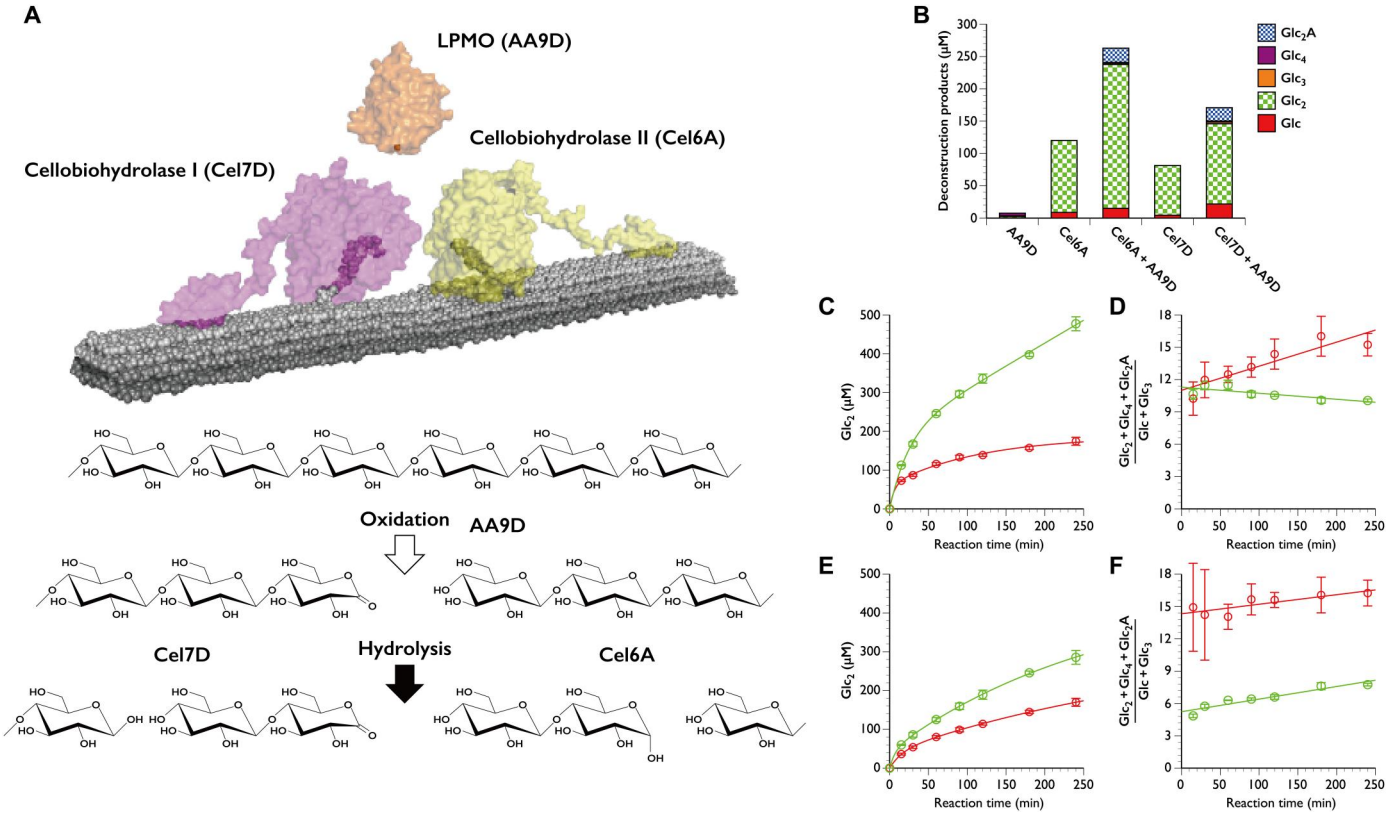

Fig. 1. AA9D and two cellobiohydrolases. (**A**) Molecular structure and activity of AA9D and the two cellobiohydrolases. Cel6A and Cel7D degrade cellulose chain from nonreducing and reducing ends, respectively, which is produced by AA9D. (**B**) Deconstruction products produced from crystalline cellulose I_α (1 mg ml^{-1}) by 1 μM cellobiohydrolases after 60-min reaction with or without 1 μM AA9D. Error bars show the SD of the total concentration of deconstruction products (from three independent measurements). (**C** and **E**) Time course of cellobiose formation and (**D** and **F**) ratio of $Glc_2 + Glc_4 + Glc_2A/Glc + Glc_3$ from crystalline cellulose I_α. Error bars show SD of data from three independent measurements. In (C) and (D), red circle, Cel6A; green circle, Cel6A with AA9D; in (E) and (F), red circle, Cel7D; green circle, Cel7D with AA9D.

RESULTS

Synergistic effects of the two CBHs and AA9D

To examine the synergistic effects between cellulases and AA9D, crystalline cellulose I_α was depolymerized by Cel6A or Cel7D in the presence or absence of AA9D and ascorbate. As shown in Fig. 1B, product formation by Cel6A or Cel7D with AA9D and ascorbate was 2.2 and 2.1 times higher than that by Cel6A or Cel7D alone, respectively. Although AA9D alone produced cello-oligosaccharides, Glc_2, Glc_3, Glc_4, and Glc_5, and oxidized cello-oligosaccharides, Glc_4A, Glc_5A, and likely Glc_6A, from crystalline cellulose I_α (fig. S1), the total amount of product was small (9.3 ± 0.4 μM in a 60-min reaction), and AA9D alone without ascorbate had no effect on the activity of Cel6A and Cel7D (fig. S2), indicating that AA9D promotes the activity of CBHs via its oxidative activity, but not via a protein-protein interaction.

As shown in Fig. 1 (C and E) and fig. S3, AA9D enhances product formation by CBHs from the beginning of the reaction. Because Glc_2 is produced mainly through processive hydrolysis, whereas Glc and Glc_3 are primary products released at the initial hydrolysis events in the reaction of CBH, the exo/endo ratio including processivity can be estimated as the ratio of $Glc_2/(Glc + Glc_3)$ (*29*). However, in the present case, Glc_2A and Glc_4 are also produced in the presence of AA9D. The ratio of even/odd oligosaccharides was calculated and plotted in Fig. 1 (D and F). No oxidized cello-oligosaccharide other than Glc_2A was detected. Cel6A and Cel7D showed somewhat different behavior; i.e., the even/odd ratio gradually increases with time for Cel6A while it was slightly increased for Cel7D, whereas in the presence of AA9D, the even/odd ratio gradually decreased with reaction time for Cel6A but remained slightly increased for Cel7D. The ratio was above 15 when the CBHs alone were used but was less than 11 for Cel6A (Fig. 1D) and less than 7 for Cel7D (Fig. 1F) in the presence of AA9D.

Change of deconstruction products with increase of AA9D concentration

We examined the deconstruction product amounts and the even/odd products ratio after reaction of AA9D (0.01 to 2.0 μM) and 1 μM Cel6A or Cel7D. As shown in Fig. 2A, increasing AA9D concentration increased the amount of deconstruction products in the case of Cel6A, whereas an increase was observed only at low concentrations of AA9D, and addition of AA9D above 0.05 μM had no further effect in the case of Cel7D (Fig. 2B). As for the even/odd products ratio, it was almost constant at around 10 in the combination with Cel6A (Fig. 2C), while in the case of Cel7D, it gradually

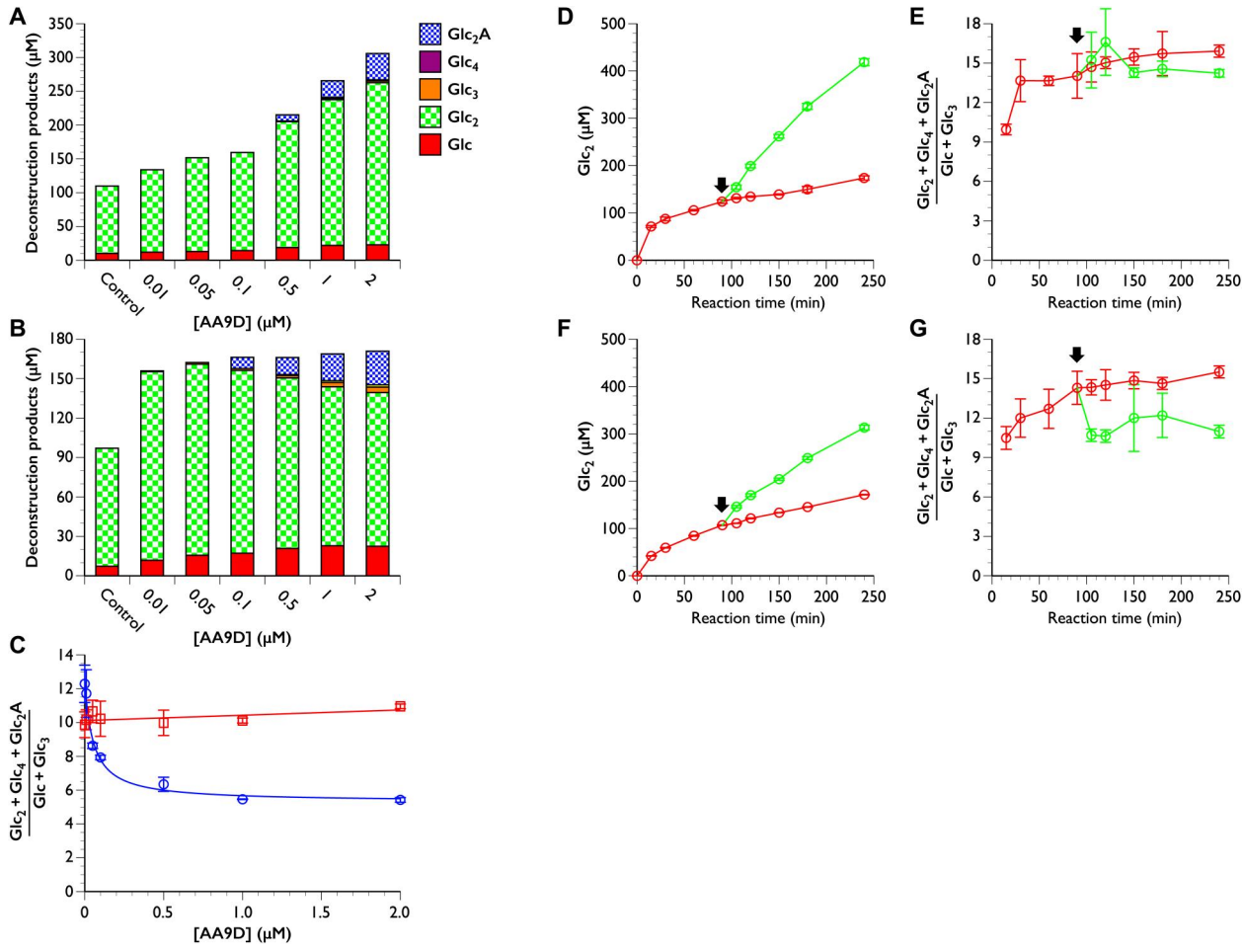

Fig. 2. Synergy between AA9D and the two cellobiohydrolases. (**A** to **C**) Concentration dependence of the effect of AA9D on crystalline cellulose I_α degradation by the two cellobiohydrolases. (A) Amount of deconstruction products when Cel6A is combined with AA9D. Deconstruction products generated from crystalline cellulose I_α (1 mg ml^{-1}) by 1 μM Cel6A after reaction in the presence of 0 to 2 μM AA9D for 60 min. (B) Amount of deconstruction products when Cel7D is combined with AA9D. Deconstruction products generated from crystalline cellulose I_α (1 mg ml^{-1}) by 1 μM Cel7D after reaction in the presence of 0 to 2 μM AA9D for 60 min. (C) Ratio of $Glc_2 + Glc_4 + Glc_2A/Glc + Glc_3$ from crystalline cellulose I_α. Red square, 1 μM Cel6A in the presence of 0 to 2 μM AA9D; blue circle, 1 μM Cel7D with 0 to 2 μM AA9D. Error bars show SD of data from three independent measurements. (**D** to **G**) Effect of adding AA9D during the reaction of the two cellobiohydrolases. (D and F) Time course of cellobiose formation and (E and G) ratio of $Glc_2 + Glc_4 + Glc_2A/Glc + Glc_3$ formed from crystalline cellulose I_α. AA9D was added at the time indicated by the black arrow (reaction time, 90 min). Error bars show SD for data from three independent measurements. In (D) and (E), red circle, 1 μM Cel6A; green circle, 1 μM Cel6A with 2 μM AA9D; in (F) and (G), red circle, 1 μM Cel7D; green circle, 1 μM Cel7D with 0.05 μM AA9D.

decreased from 12 to 6 with increasing concentration of AA9D (Fig. 2C).

The effect of adding AA9D to Cel6A or Cel7D in the middle of the reaction, i.e., 90 min after initiation of the reaction, was then tested (Fig. 2, D to G, and fig. S4). Immediately after AA9D addition, the amount of deconstruction products (mainly Glc_2) increased, as shown in Fig. 2 (D and F). Glc_2A was formed only after the addition of AA9D (fig. S4, D and H), and no other oxidized cello-oligosaccharide was detected. As shown in Fig. 2E, the values of even/odd ratio for Cel6A with and without AA9D were similar, while for Cel7D, the ratio dropped from 15 in the absence of AA9D to about 11 in its presence (Fig. 2G).

MD simulation

The structural impact of AA9D activity on the crystalline cellulose surface was evaluated by analyzing MD trajectories of intact and oxidatively cleaved cellulose surfaces. To prepare a crystalline cellulose surface for analysis, five, six, and seven cello-oligo chains consisting of 14-mer glucose residues were stacked in three layers in the cellulose I_α orientation (fig. S5), in the same manner as in our previous work (*30*–*32*). The middle chain on the crystalline cellulose surface was modeled as being oxidatively cleaved at the glycosidic bond between the seventh and eighth Glc, mimicking AA9D activity, and this structure was compared with the intact chain control simulation. AA9D oxidizes the C-1 position of the seventh Glc to form either a glucono-δ-lactone or a gluconic acid, depending on subsequent hydrolysis in solution, and we therefore simulated both states. Figure 3 and movies S1 to S3 show the MD simulation results.

The oxidation of the seventh Glc has a substantial impact on the local cellulose structure. The deviation from the crystal structure [measured as root mean square deviation (RMSD)], the fluctuation

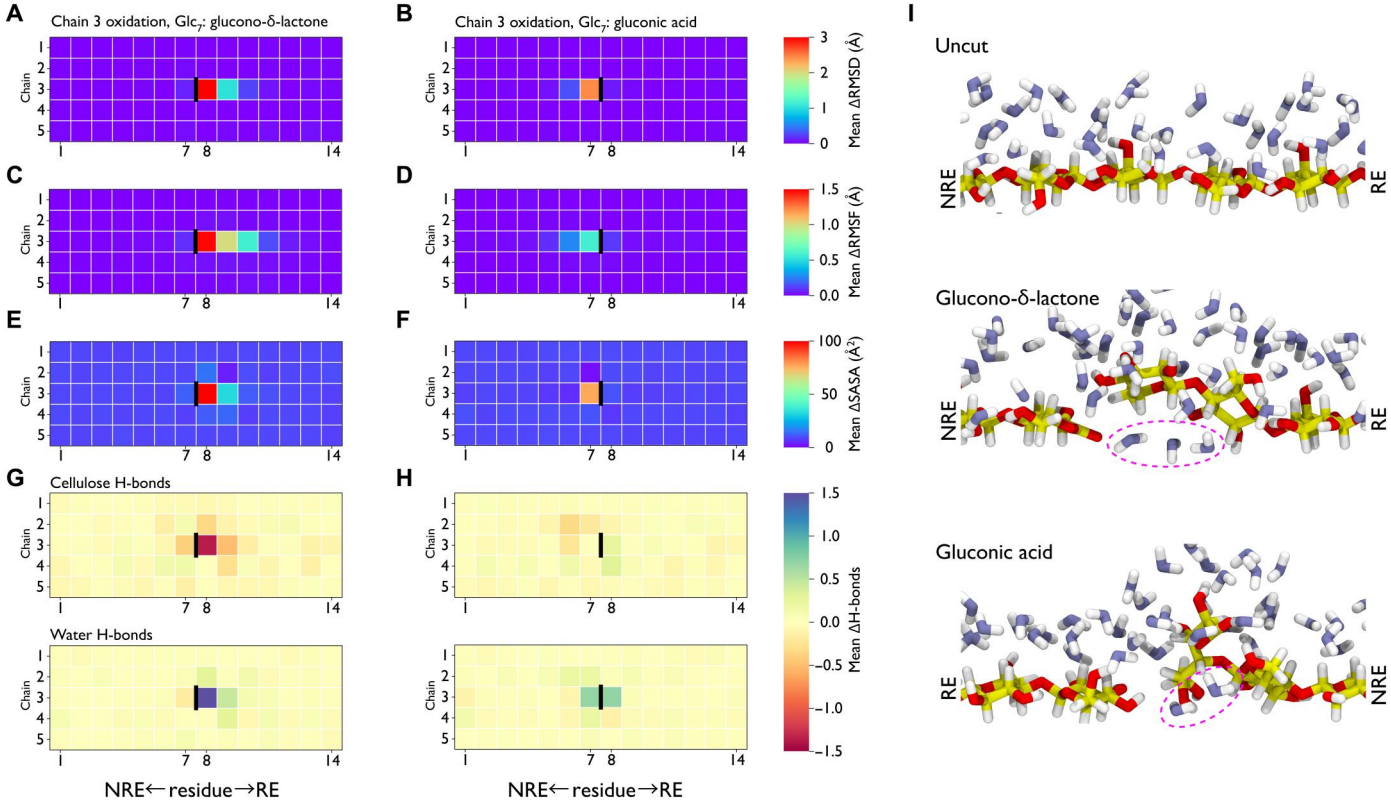

Fig. 3. MD simulation of the effect of glycosidic bond cleavage by AA9D on the hydrophobic surface of cellulose. (**A** to **H**) Results of simulating RMSD, RMSF, SASA, and H-bonds when the glycosidic bond between glucose residues 7 and 8 of the third chain is cleaved, indicated by a vertical black line. The vertical axis shows the number of chains (1 to 5), and the horizontal axis shows the glucose residue at the nonreducing end (NRE) side as 1 and the glucose residue at the reducing end (RE) side as 14. (A to H) Changes in glycosidic bond cleavage relative to the intact control; (A and B) the time averaged RMSD change for the oxidatively cleaved surface when compared with the intact chains; (C and D) RMSF change for the oxidatively cleaved surface when compared with the intact chains; (E and F) change in SASA after the middle chain is oxidatively cleaved. Top panels of (G) and (H) show the change in hydrogen bonds within the cellulose fibrils after oxidative cleavage. Bottom panels of (G) and (H) quantify the change in hydrogen bonding between cellulose and water molecules on a per-residue basis. (A), (C), (E), and (G) show simulation results when the seventh residue is glucono-δ-lactone, while (B), (D), (F), and (H) show simulation results when the seventh residue is gluconic acid. (**I**) Snapshots of water molecules near the central chain for the three tested states. In the intact state, all water molecules (blue, oxygens; white, hydrogens) can access the primary surface. For clarity, only the central chain (yellow, carbons; red, oxygens; white hydrogens) and water molecules within 4 Å of this chain are shown. Some water molecules end the MD simulation underneath the original surface and are highlighted by a dashed pink oval.

[measured as root mean square fluctuation (RMSF)], and the solvent-accessible surface area (SASA) are all increased adjacent to the bond cleavage site, as compared with the intact crystal structure (Fig. 3, A to F, and movies S2 and S3).

In the 1-μs MD trajectory, the identity of the most exposed chain depends on the oxidation chemistry. When the seventh Glc is transformed to glucono-δ-lactone, the eighth Glc nonreducing end chain is exposed on the hydrophobic surface (Fig. 3, A, C, and E, and movie S2). Conversely, when the seventh Glc residue is transformed to gluconic acid, the gluconic acid on the reducing end chain is exposed on the hydrophobic surface (Fig. 3, B, D, and F, and movie S3).

Next, we calculated the change in the amount of hydrogen bonds of Glc residues forming the hydrophobic surface (Fig. 3, G and H). MD analysis indicated that when the seventh residue is glucono-δ-lactone, hydrogen bonding between the eighth Glc residue and other Glc residues constituting the cellulose surface is decreased, while hydrogen bonding with water is increased (Fig. 3G). However, when the seventh residue is gluconic acid (Fig. 3H), little change is observed in the hydrogen bonds between the cellulose chains, while the hydrogen bonds between the seventh and eighth residues and water are increased. Figure 3I shows snapshots of intact cellulose chain and the chain attacked by AA9D, as well as free water molecules around them. It can be seen that more water molecules are attracted to the newly formed chain ends compared to the intact chain. In addition, the presence of water molecules that penetrate between the newly formed ends and crystalline cellulose surface was simulated. Thus, the MD analysis indicates that cleavage of the glycosidic bond by AA9D attracts water molecules onto the hydrophobic surface of crystalline cellulose, solvating cellulose chains, and exposing them to the solution. Furthermore, it is considered that water molecules penetrate between the newly formed chain terminals and the crystalline cellulose surface, disturb hydrogen bonds, and promote cellulose surface decrystallization.

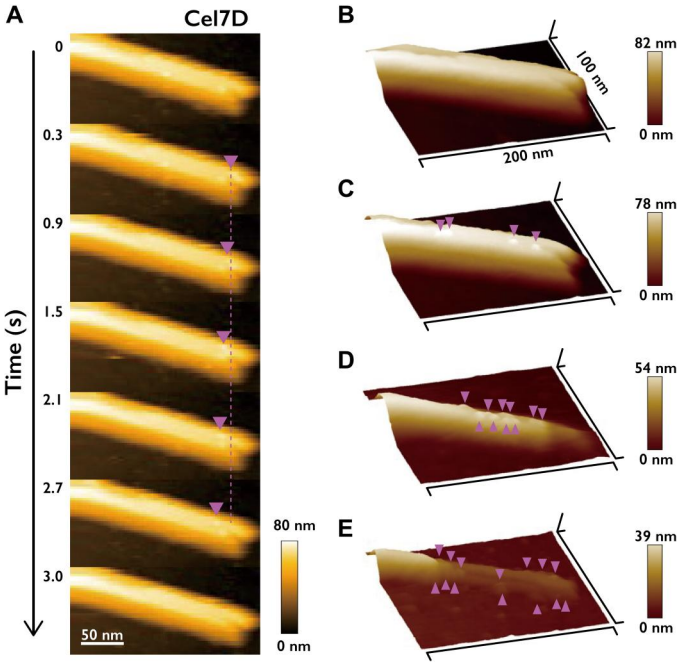

Fig. 4. HS-AFM images of Cel7D. Positions of Cel7D molecules are indicated by magenta arrowheads. (**A**) Real-time observation of crystalline cellulose I_α incubated with 1 μM Cel7D by means of HS-AFM. The time interval between images is 0.3 s (200 × 100 nm^2, 120 × 60 pixels). (**B**) Crystalline cellulose I_α before enzyme addition. (**C**) Image at 4.5 min after the addition of Cel7D. (**D** and **E**) Images at 15.0 min (D) and 27.0 min (E) after the addition of 0.5 μM AA9D following incubation with Cel7D. The degradation of crystalline cellulose I_α by Cel7D and AA9D increased with increasing reaction time.

HS-AFM observation of synergistic interaction of Cel7D and AA9D

As shown in Fig. 4A, unidirectional movement of Cel7D molecules on the surface of crystalline cellulose I_α was observed by HS-AFM, while such moving molecules could not be observed in the case of Cel6A, possibly because of its low degree of processivity (*33*).

Moreover, in the case of AA9D, even adsorbed molecules on the cellulose surface could not be observed. When Cel7D was loaded alone, the molecules mainly moved in a specific part of the substrate as shown in Fig. 4C and movie S4, upper panel. In movie S4, , molecules with processive movement were observed mainly on the lateral side of the cellulose fiber. However, after addition of AA9D, the number of Cel7D molecules moving on the surface of cellulose I_α apparently increased, and the molecules moved over more diverse sites on the surface of cellulose I_α as shown in Fig. 4 (D and E) and movie S4, lower panel. In movie S4, lower panel, observed molecules move not only on the side of the cellulose fiber but also in the center.

The movement of Cel7D molecules before and after the addition of AA9D was then analyzed statistically (fig. S6) and the obtained parameters are listed in Table 1.

Figure S6C shows a histogram of the velocities of Cel7D (n = 89), exhibiting a Gaussian distribution with a mean ± SD of 9.4 ± 4.1 nm s^{-1}. Figure S6E shows a histogram of the distribution of the duration of movement of Cel7D molecules; the time constant ± SE was 0.4 ± 0.1 s. From the velocity and the time constant, the processivity of Cel7D for cellulose I_α was estimated to be 4.04 successive reactions, taking the length of the cellobiose repeating unit as 1.0 nm in crystalline cellulose (*34*). We also analyzed the molecular movements of Cel7D in the presence of AA9D and estimated the kinetic parameters. Figure S6B shows the time courses for Cel7D (n = 314), indicating that Cel7D molecules were mobile for longer in the presence of AA9D than in its absence (fig. S6A). The velocities of Cel7D molecules showed a Gaussian distribution with a mean ± SD of 9.4 ± 3.3 nm s^{-1}, which is the same as the velocity of Cel7D alone (fig. S6D). However, as shown in fig. S6F, the time constant ± SE of the duration of Cel7D molecules on the surface was 1.5 ± 0.2 s, corresponding to 14.4 reactions, which is 3.6 times longer than in the absence of AA9D. On the basis of the HS-AFM observations, we analyzed whether there is a difference in the amount of Cel7D adsorbed on cellulose I_α before and after the addition of AA9D (Fig. 5).

After the addition of Cel7D, the count was started from the point where the molecules were adsorbed for 0.6 s (two frames of HS-AFM images) or longer on a section of the cellulose surface (Fig. 5A; one section is 140 nm by 60 nm). The number of Cel7D molecules adsorbed was counted before and after the addition of AA9D, 383.1 s after the start time (Fig. 5B). In addition, to confirm that the suspending action did not affect Cel7D adsorption onto the substrate, we carried out mixing by a micropipette (after 190.2 to 217.8 s from the start) during the observation when Cel7D was added alone. AA9D was added at 383.1 to 406.2 s after the start of the reaction. Figure 5B shows the numbers of Cel7D molecules adsorbed on a section of the cellulose surface at every 0.3 s from the start of the reaction until 761.1 s. As shown in Fig. 5C, Cel7D molecules adhered to a limited area on the cellulose surface before the addition of AA9D, possibly attacking preexisting chain ends. However, after the addition of AA9D, more adhesion sites were observed over the cellulose surface (Fig. 5D). The average number of Cel7D molecules adsorbed on the substrate from the start to 189.6 s was 0.023 molecules nm^{-2} s^{-1}. The average number of Cel7D molecules adsorbed on the substrate surface for 164.7 s from the mixing to before the addition of AA9D was 0.020 molecules nm^{-2} s^{-1}. Thus, the suspending action itself has essentially no effect on the adsorption rate of Cel7D molecules on the substrate. However, the average number of Cel7D molecules adsorbed on the substrate surface at 354.6 s after the addition of AA9D was 0.042 molecules nm^{-2} s^{-1}. Thus, the number of adsorbed Cel7D molecules was doubled by the addition of AA9D. The number of Cel7D molecules that showed processive reaction also increased from 89 to 156 before and after the addition of AA9D. Moreover, the processivity of Cel7D increased after the addition of AA9D (Table 1), suggesting that more Cel7D molecules remained on the cellulose surface for a longer period of time. These results suggested that the activity of AA9D not only enhances the processivity of Cel7D but also generates a substrate surface on which Cel7D is more easily adsorbed.

DISCUSSION

In the present study, we tested the synergistic effect of degradation of crystalline cellulose I_α by AA9D and Cel7D or Cel6A, all from the wood-rotting fungus *P. chrysosporium*. When the amount of AA9D was increased, the amount of deconstruction products generated by Cel6A was clearly increased, while the even/odd products ratio remained almost constant (Fig. 2, A and C). This is presumably

Table 1. Comparison of statistical parameters of Cel7D and Cel7D with AA9D.

Enzyme(s)	Dissociation rate constant (s^{-1})*	Half-life of movement (s)†	Average velocity (nm s^{-1})‡	Calculated processivity (number of reactions)
Cel7D	1.61 ± 0.23	0.4 ± 0.1	9.4 ± 4.1	4.04
Cel7D with AA9D	0.46 ± 0.06	1.5 ± 0.2	9.4 ± 3.3	14.4

*The values are rate constant ± SE of the fitting with exponential decay. †The values are time constant ± SE of the fitting with exponential decay. ‡The values are means ± SD for a Gaussian distribution.

because the C1-oxidizing activity of AA9D increases the activity of Cel6A by producing newly formed nonreducing ends. In the case of Cel7D, addition of AA9D also enhanced Cel7D activity by 1.8-fold compared to that without AA9D (Fig. 2B). However, the amount of deconstruction products did not increase when the concentration of AA9D was further increased. In addition, the even/odd products ratio, an indicator of exo/endo ratio and processivity (Fig. 2C), was markedly decreased for Cel7D, which should be due to a difference in the effect of oxidation of the C-1 hydroxyl group on the two CBHs. However, the increased activity of both enzymes at low concentrations of LPMO without formation of oxidative products cannot be well explained simply in terms of an increase in the number of chain ends.

There are several reports indicating that LPMO oxidation of the Glc C-1 hydroxyl group shows little or no synergy with GH7 CBH activity. Zhou *et al.* (*16*) tested the synergies between LPMO from *Myceliophthora thermophila* (*Mt*LPMO9L) and GH7 CBH from *Trichoderma longibrachiatum* or GH6 CBH using phosphoric acid–swollen cellulose (PASC) and Avicel as substrates and found no synergy in the combination of *Mt*LPMO9L and GH7 CBH for Avicel degradation; apparent synergy was observed only at a ratio of LPMO:CBH = 1:10 for PASC degradation. At a ratio of 10:1, activity toward both Avicel and PASC was reduced. However, synergies were observed toward both Avicel and PASC when *Mt*LPMO9L and GH6 CBH were mixed at a ratio of 10:1. Tokin *et al.* (*17*) examined synergism of three LPMOs (*Ta*AA9A from *Thermoascus aurantiacus*, *Ls*AA9A from *Lentinus similis*, and *Tt*AA9E from *Thielavia terrestris*) with two CBHs from *Trichoderma reesei* (*Tr*Cel6A and *Tr*Cel7A) for deconstruction of PASC or Avicel. When LPMOs oxidizing both C-1/C-4 hydroxyl groups (*Ta*AA9A and *Ls*AA9A) were used, synergies were found with *Tr*Cel6A and *Tr*Cel7A for both PASC and Avicel degradation. However, *Tt*AA9E, which oxidizes the C-1 hydroxyl group of Glc, showed synergism only with *Tr*Cel6A; the activity of *Tr*Cel7A remained the same or was reduced in the presence of *Tt*AA9E. These reports indicate that the combination of LPMO oxidizing the C-1 hydroxyl group and GH7 CBHs has only a limited effect on cellulose degradation, whereas the combination of LPMO and GH6 CBHs exhibits synergistically increased activity. It should be noted that our study and the other reports differ in the substrate used to examine the synergistic effects of CBHs and LPMO.

The results obtained in this work with Cel7D and AA9D are in contrast to the previous finding that the activity of *Tr*Cel7A was decreased by LPMO-mediated oxidation of the C-1 hydroxyl group (*17*). In a previous study, HS-AFM observations revealed that *Tr*Cel7A shows stronger processivity than Cel7D, probably due to the extended loop covering the active cleft in *Tr*Cel7A (*25*). The action of *Tr*Cel7A, which exhibits a high degree of processivity, is hindered by LPMO oxidizing the C-1 hydroxyl group, while Cel7D, which has lower processivity than *Tr*Cel7A, is not inhibited but shows endo-initiation activity, and consequently, there is no decrease in total depolymerization activity, as shown in Fig. 2 (B and C). Considering the results of prior MD studies, which indicated that the processive movement of *Tr*Cel7A is inhibited when the reducing end of the cellulose chain is oxidized to gluconic acid (*32*), as well as our previous report that oxidation of the C-1 hydroxyl group in cellobiose by CDH relieves product inhibition of Cel7D (*35*), we hypothesize that oxidation of the reducing end inhibits the process of loading the substrate chain into the active site and/or processive movement of the catalytic domain during hydrolysis of GH7 CBHs. In contrast, GH6 CBHs start their reaction at the nonreducing end of the cellulose chain. Because AA9D activity exposes unmodified glucose residues at the nonreducing end, AA9D may directly lead to increased accessibility of cellulose chains to GH6 CBHs. Christensen *et al.* (*36*) reported that the association (k_{on}) and dissociation (k_{off}) constants of *Tr*Cel6A are 20 to 50 times higher than those of *Tr*Cel7A, supporting the idea that Cel6A attacks sites generated by the oxidation more effectively than does Cel7D.

The MD simulation indicates that oxidation by AA9D results in exposure of the nonreducing-end Glc residue or the reducing-end residue on the surface depending on the terminal structure, namely, glucono-δ-lactone or gluconic acid, respectively. The oxidative cleavage not only increases the solvation of the newly generated chain ends but also disturbs the crystalline cellulose surface by disrupting hydrogen bonds, which likely promotes cellulose hydrolysis by CBHs. We have also previously succeeded in visualizing cellulase molecules on the surface of crystalline cellulose I_α by means of HS-AFM (*37*), and therefore, we applied this technique to visualize the synergistic action of Cel7D and AA9D. The number of observed Cel7D molecules increased after the addition of a low concentration of AA9D, indicating that AA9D creates more access points for Cel7D on the substrate surface. Eibinger *et al.* (*38*) proposed that oxidation of the C-1 hydroxyl group by LPMO increases the amount of *Tr*Cel7A molecules adsorbed on a crystalline cellulose surface and increases their processivity. We statistically analyzed the present observations, and the results established that movements of Cel7D molecules on the substrate surface are longer in the presence of AA9D (Table 1 and fig. S6). The greater half-life of movement of Cel7D in the presence of AA9D indicate that the substrate surface is more susceptible to attack by Cel7D, and the cellulose chain is more easily retained in the active site tunnel.

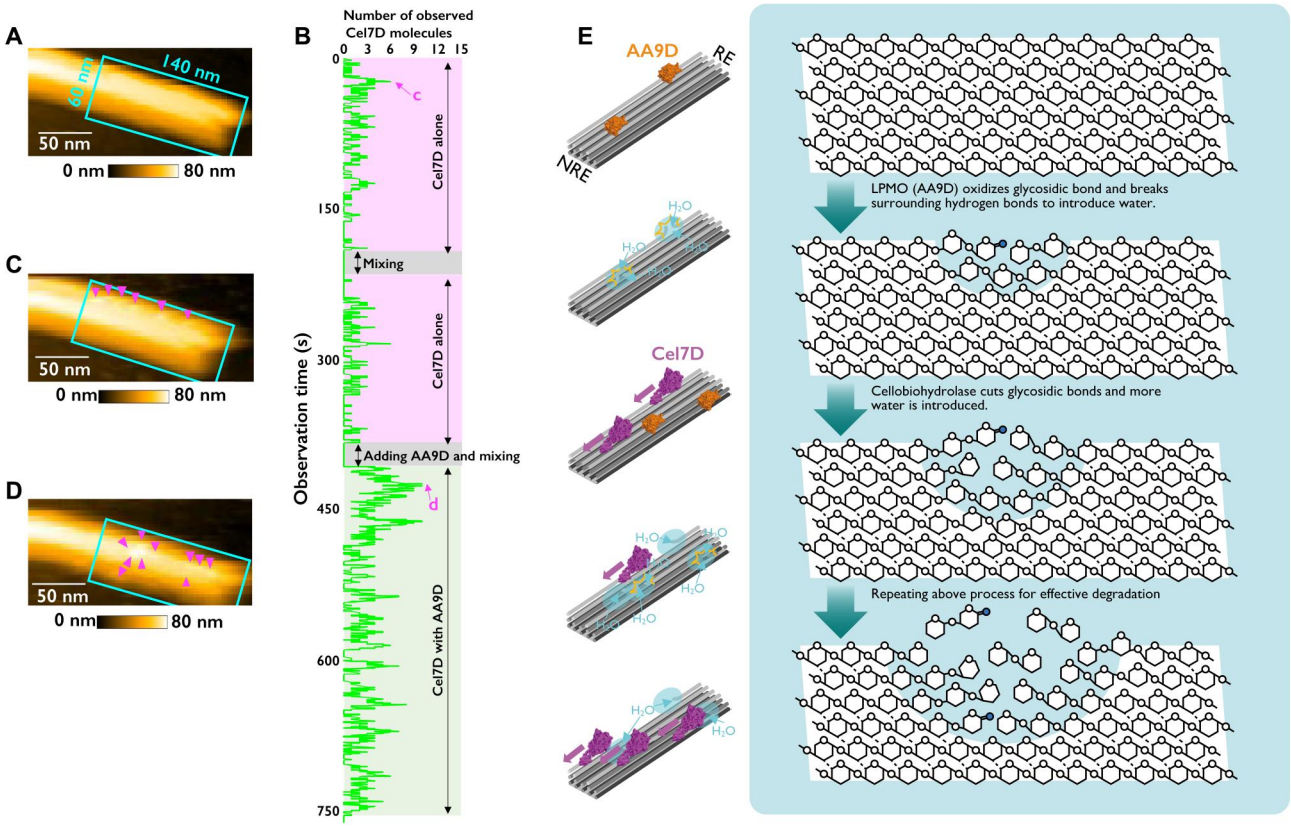

Fig. 5. Synergistic action of Cel7D and AA9D from *P. chrysosporium* in degrading crystalline cellulose I_α. (**A**) Counting area of the crystalline cellulose I_α surface observed by HS-AFM. (**B**) Real-time observation of the number of Cel7D molecules attached to and detached from the surface of cellulose I_α. Reaction by 1 μM Cel7D. The mixing is indicated by the gray background. Arrow "c" is the point at which the image (**C**) was obtained. At 380 s after the start of counting, 0.5 μM AA9D was added and mixed; the timing is indicated by a gray background. Arrow "d" is the point at which image (**D**) was obtained. (C) Image containing the most molecules in the counting area in the presence of Cel7D alone. Positions of Cel7D molecules are marked by magenta arrowheads. This image is taken from movie S4, upper panel. (D) Image containing the most molecules in the counting area in the presence of Cel7D with AA9D. Positions of Cel7D molecules are marked by magenta arrowheads. This image is taken from movie S4, lower panel. (**E**) Synergistic mechanism of cellulolytic activity of Cel7D and AA9D. AA9D acts on crystalline cellulose to generate more cellulose chain ends and Cel7D conducts processive reaction from these chain ends. In addition, the chain ends generated by AA9D activity attract water molecules onto the hydrophobic surface of cellulose and thereby increase the endo-type reaction of Cel7D to promote cellulase activity. These two functions of AA9D synergistically promote the cellulolytic reaction of Cel7D.

The biochemical experiments revealed that the addition of AA9D enhanced the "velocity of product formation," which takes account of processivity and the endo/exo ratio, by Cel7D. Although an endo-type reaction could not be distinguished by HS-AFM, AA9D enhances the processivity of Cel7D, while the even/odd ratio is lowered by AA9D, indicating an increased likelihood of endo-type reaction of Cel7D. The increased endo activity indicates that the activity of AA9D not only creates cellulose chain terminals by oxidation but also modifies the cellulose surface.

On the basis of the MD analysis and the experimental results, we propose a mechanistic model for synergistic degradation of crystalline cellulose by AA9D and Cel7D (Fig. 5E). AA9D adsorbed on the hydrophobic surface of crystalline cellulose cleaves the glycosidic bonds within cellulose chains on the surface. Glc at the nonreducing end or gluconic acid at the reducing end is exposed at the cleaved site, and water molecules solvate residues near the cleavage site. After spontaneous hydrolysis of glucono-δ-lactone to gluconic acid, Cel7D captures exposed gluconic acid residues and initiates processive hydrolysis. If Cel6A arrives before glucono-δ-lactone hydrolysis, the enzyme would find an exposed nonreducing chain end suitable for processive hydrolysis. Furthermore, the existence of water molecules that penetrate between the newly formed terminal and the crystalline cellulose has been predicted, and it is considered that such water molecules would promote decrystallization of the surface of the crystalline cellulose, making it more vulnerable to attack by CBHs. The decrystallized surface hinders the processive action of CBHs, but if the endo activity of CBHs is sufficient, the CBHs generate chain ends and create more decomposable surfaces on their own.

The LPMO examined in the present study, AA9D, is classified as a monooxygenase oxidizing the C-1 hydroxyl group of Glc, but there are also LPMOs able to oxidize the C-4 hydroxyl group (*39*) and both C-1/C-4 hydroxyl groups (*40*). Thus, the synergy between LPMOs and CBHs may change depending on the precise combination of enzymes. To date, there are few reports on the synergistic effects of LPMO and EG (*41*, *42*), warranting further research to develop LPMOs as enzymes for enhancing the degradability of insoluble polysaccharides.

MATERIALS AND METHODS

Materials

Crystalline cellulose I_α was prepared from green algae *Cladophora* spp. according to the reported method (*28*). Cello-oligosaccharides were acquired from Seikagaku Kogyo. Calcium cellobionate was purchased from ICN Biomedicals.

Expression and purification of AA9D, Cel6A, and Cel7D from *P. chrysosporium*

Expression and purification of recombinant AA9D were carried out as described previously (*26*). Cel6A was a purified recombinant enzyme preparation from *Pichia pastoris* (*43*). Cel7D was purified from the supernatant of *P. chrysosporium* strain K-3 grown on Kremer and Wood medium containing 2% cellulose as the sole carbon source as described previously (*25*).

Enzyme assay

Enzyme activity toward crystalline cellulose I_α was determined in a 150-μl reaction mixture containing 50 mM sodium acetate buffer (pH 5.0), 1.0 mM ascorbate, substrate (1.0 mg ml^{-1}), and a designated concentration (micromolar) of enzyme at 35°C. The reaction was stopped by heating the sample to 98°C for 5 min. Deconstruction products formed from cellulose I_α were separated from the reaction mixture by using a 0.22-μm Durapore polyvinylidene difluoride membrane filter (MultiScreen $_{HTS}$-GV, Merck Millipore) and were analyzed by high-performance liquid chromatography (LC-2000 series, Jasco) using a Corona-charged aerosol detector (Corona CAD, ESA Biosciences) and a prepacked Shodex Asahipak NH2P-50 column (4.6 by 250 mm, Showa Denko K. K.). The eluent was 50 mM $CH_3COO(NH_4)$ (pH 6.0), containing a linear gradient of CH_3CN from 60 to 55% for 5 min, fixed at 55% for 3 min, fixed at 25% for 20 min, and fixed at 60% for 5 min. The column was kept at 40°C and eluted at 1.0 ml min^{-1}. Glucose (Glc), cellobiose (Glc_2), cellotriose (Glc_3), cellotetraose (Glc_4), cellopentaose (Glc_5), and cellobionic acid (Glc_2A) were identified and quantitated by comparing the retention times and peak areas with those of authentic standards. Cellotrionic acid (Glc_3A), cellotetraonic acid (Glc_4A), and cellopentaonic acid (Glc_5A) were identified by comparing the retention times with those of CDH-treated cello-oligosaccharides (*44*). AA9D addition during the reaction of CBHs was performed as follows. Add the remaining 1.5 μl to prepare a 150-μl reaction solution that will give a final concentration of 1.0 mg ml^{-1} substrate, 1.0 μM Cel6A or Cel7D, 50 mM sodium acetate buffer (pH 5.0), and 1.0 mM ascorbate, which was incubated at 35°C for 90 min. Then, 1.5 μl of AA9D (to a final concentration of 2.0 μM for Cel6A or 0.05 μM for Cel7D) or water was added and incubated for each time. The reaction was stopped by heating the sample to 98°C for 5 min. For the reaction solution before 90-min incubation, incubating 148.5-μl of reaction mixture until each time then the reaction was stopped at 98°C for 5 min, and 1.5 μl of water was added to prepare a 150-μl reaction solution.

HS-AFM observation

Moving molecules of Cel7D were observed by HS-AFM, similar to previous reports (*25*, *33*, *37*, *45*–*47*). A suspension (1 mg ml^{-1}) of highly crystalline cellulose I_α was dropped on a highly oriented pyrolytic graphite stage and incubated at 25°C for 10 min. The stage was rinsed with 50 mM sodium acetate buffer (pH 5.0) and 1 mM ascorbate to remove unbound cellulose I_α and set on the instrument, and then 78 μl of the same buffer was added, followed by 2 μl of 40 μM Cel7D solution. We analyzed molecules whose movement started and ended in the observation area. When AA9D was included, 2 μl of 20 μM AA9D was added to the system.

For statistical analysis of the moving velocities of individual Cel7D molecules, semi-automatic tracking of each molecule on the kymograph was carried out (*33*, *47*). The moving velocities of cellulase molecules were obtained by IGOR Pro 6 (WaveMetrics, Portland, OR) and fitted to a Gaussian distribution. Histogram data were tested for normality using the Shapiro-Wilk test (Prism7, GraphPad). Values satisfied the Shapiro-Wilk test, confirming a normal distribution ($P \geq 0.05$). Adsorption times of molecules were calculated from the number of frames in which the molecules were observed. The plots of numbers of molecules in each range of adsorption time were fitted by a single exponential function, and a time constant was estimated (*25*, *33*, *47*).

The time course of the number of Cel7D molecules attached to the surface of cellulose I_α was determined as follows. The number of molecules adhering to the surface was determined every 0.3 s. Molecules remaining for 0.6 s or more were counted as adsorbed. Molecules that disappeared in 0.3 s were considered nonadsorbed and were not counted. The time when Cel7D was added and the first molecule remained for 0.6 s or more was used as the starting point for counting the adsorbed molecules of Cel7D alone. Then, AA9D was added, and the time at which a molecule remained for 0.6 s or more was similarly set as the starting point for counting adsorbed molecules of Cel7D in the presence of AA9D.

MD simulation

Three simulation systems were prepared to study cellulose structure after oxidative cellulose cleavage by LPMOs, following strategies outlined in our previous work on polysaccharide decrystallization (*30*–*32*, *48*), using partial cellulose microfibrils solvated in explicit water. In one system, which served as the control, all cellulose fibrils remain intact. Two additional simulations were prepared where the crystalline cellulose was oxidatively cut, leaving either a glucono-δ-lactone or gluconic acid exposed on the reducing end of the newly exposed chain termini, as shown in fig. S5. Both potential cleavages represent alternative reducing-end oxidations possible after LPMO action. To provide an accurate environment for the cut chain, additional cellulose layers were included within the simulation to monitor their fluctuations. The initial cellulose structure was taken from previously equilibrated structures. To reduce simulation cost, only three layers of cellulose were included, with the cellulose at the fibril midplane restrained in space through 1 kcal mol^{-1} $Å^{-2}$ harmonic restraints applied to the glucose rings. To emulate a longer cellulose crystal, chain ends at residues 1 and 14 were also restrained via 1 kcal mol^{-1} $Å^{-2}$ harmonic restraints applied to glucose ring atoms.

The three systems were simulated for 1000 ns using NAMD 2.13 (*49*) with the CHARMM36 force field for carbohydrates (*50*) and water (*51*), using previously parameterized force fields for oxidized cellulose (*32*). The simulations were performed in the NPT ensemble, using a Langevin thermostat (*52*) and barostat (*53*) to maintain 298 K and 1 atm, respectively. The RATTLE algorithm (*54*) was applied to hydrogens to enable 2-fs time steps. Particle mesh Ewald with 1.2 Å spacing was applied to compute long-range electrostatics (*55*), while VDW and short-range electrostatics were

switched at 10 Å and cutoff at 12 Å. The trajectories were analyzed using python-enabled VMD 1.9.3 (*56*), leveraging NumPy (*57*) and matplotlib (*58*) libraries for plotting and analysis.

Supplementary Materials

This PDF file includes:
Figs. S1 to S6

Other Supplementary Material for this manuscript includes the following:
Movies S1 to S4

View/request a protocol for this paper from *Bio-protocol*.

REFERENCES AND NOTES

1. C. M. Payne, B. C. Knott, H. B. Mayes, H. Hansson, M. E. Himmel, M. Sandgren, J. Ståhlberg, G. T. Beckham, Fungal cellulases. *Chem. Rev.* **115**, 1308–1448 (2015).
2. G. R. Hemsworth, E. M. Johnston, G. J. Davies, P. H. Walton, Lytic polysaccharide monooxygenases in biomass conversion. *Trends Biotechnol.* **33**, 747–761 (2015).
3. Z. Forsberg, M. Sørlie, D. Petrovic, G. Courtade, F. L. Aachmann, G. Vaaje-Kolstad, B. Bissaro, Å. K. Røhr, V. G. H. Eijsink, Polysaccharide degradation by lytic polysaccharide monooxygenases. *Curr. Opin. Struct. Biol.* **59**, 54–64 (2019).
4. G. Vaaje-Kolstad, B. Westereng, S. J. Horn, Z. Liu, H. Zhai, M. Sørlie, V. G. H. Eijsink, An oxidative enzyme boosting the enzymatic conversion of recalcitrant polysaccharides. *Science* **330**, 219–222 (2010).
5. L. Lo Leggio, T. J. Simmons, J. -C. N. Poulsen, K. E. H. Frandsen, G. R. Hemsworth, M. A. Stringer, P. von Freiesleben, M. Tovborg, K. S. Johansen, L. De Maria, P. V. Harris, C. -L. Soong, P. Dupree, T. Tryfona, N. Lenfant, B. Henrissat, G. J. Davies, P. H. Walton, Structure and boosting activity of a starch-degrading lytic polysaccharide monooxygenase. *Nat. Commun.* **6**, 5961 (2015).
6. M. Frommhagen, M. J. Koetsier, A. H. Westphal, J. Visser, S. W. A. Hinz, J. -P. Vinncken, W. J. H. van Berkel, M. A. Kabel, H. Gruppen, Lytic polysaccharide monooxygennases from *Myceliophthora thermophila* C1 differ in substrate preference and reducing agent specificity. *Biotechnol. Biofuels* **9**, 1–17 (2016).
7. B. Westereng, D. Cannella, J. Wittrup Agger, H. Jørgensen, M. Larsen Andersen, V. G. H. Eijsink, C. Felby, Enzymatic cellulose oxidation is linked to lignin by long-range electron transfer. *Sci. Rep.* **5**, 18561 (2015).
8. C. M. Phillips, W. T. Beeson, J. H. Cate, A. S. Marletta, Cellobiose dehydrogenase and a copper-dependent polysaccharide monooxygenase potentiate cellulose degradation by *Neurospora crassa*. *ACS Chem. Biol.* **6**, 1399–1406 (2011).
9. S. Garajova, Y. Mathieu, M. R. Beccia, C. Bennati-Granier, F. Biaso, M. Fanuel, D. Ropartz, B. Guigliarelli, E. Record, H. Rogniaux, B. Henrissat, J. -G. Berrin, Single-domain flavoenzymes trigger lytic polysaccharide monooxygenases for oxidative degradation of cellulose. *Sci. Rep.* **6**, 28276 (2016).
10. A. Várnai, K. Umezawa, M. Yoshida, V. G. H. Eijisink, The pyrroloquinoline-quinone dependent pyranose dehydrogenase from *Coprinopsis cinerea* (CcPDH) drives lytic polysaccharide monooxygenase (LPMO) action. *Appl. Environ. Microbiol.* **84**, e00156-18 (2018).
11. D. Canella, K. B. Möllers, N. U. Frigaard, P. E. Jensen, M. J. Bjerrum, K. S. Johansen, C. Felby, Light-driven oxidation of polysaccharides by photosynthetic pigments and a metalloenzyme. *Nat. Commun.* **7**, 11134 (2016).
12. B. Bissaro, Å. K. Røhr, G. Müller, P. Chylenski, M. Skaugen, Z. Forsberg, S. J. Horn, G. Vaaje-Kolstad, V. G. H. Eijsink, Oxidative cleavage of polysaccharides by monocopper enzymes depends on H_2O_2. *Nat. Chem. Biol.* **13**, 1123–1128 (2017).
13. R. J. Quinlan, M. D. Sweeney, L. Lo Leggio, H. Otten, J. N. Poulsen, K. S. Johansen, K. B. Krogh, C. I. Jørgensen, M. Tovborg, A. Anthonsen, T. Tryfona, C. P. Walter, P. Dupree, F. Xu, G. J. Davies, P. H. Walton, Insights into the oxidative degradation of cellulose by a copper metalloenzyme that exploits biomass components. *Proc. Natl. Acad. Sci. U.S.A.* **108**, 15079–15084 (2011).
14. M. Eibinger, T. Ganner, P. Bubner, S. Rosker, D. Kracher, D. Haltrich, R. Ludwig, H. Plank, B. Nidetzky, Cellulose surface degradation by a lytic polysaccharide monooxygenase and its effect on cellulase hydrolytic efficiency. *J. Biol. Chem.* **289**, 35929–35938 (2014).
15. B. Song, B. Li, X. Wang, W. Shen, S. Park, C. Collings, A. Feng, S. J. Smith, J. D. Walton, S. Y. Ding, Real-time imaging reveals that lytic polysaccharide monooxygenase promotes cellulase activity by increasing cellulose accessibility. *Biotechnol. Biofuels* **11**, 41 (2018).
16. H. Zhou, T. Li, Z. Yu, J. Ju, H. Zhang, H. Tan, K. Li, H. Yin, A lytic polysaccharide monooxygenase from *Myceliophthora thermophila* and its synergism with cellobiohydrolases in cellulose hydrolysis. *Int. J. Biol. Macromol.* **139**, 570–576 (2019).
17. R. Tokin, J. Ø. Ipsen, P. Westh, K. S. Johansen, The synergy between LPMOs and cellulases in enzymatic saccharification of cellulose is both enzyme- and substrate-dependent. *Biotechnol. Lett.* **42**, 1975–1984 (2020).
18. J. Hu, V. Arantes, A. Pribowo, K. Gourlay, J. N. Saddler, Substrate factors that influence the synergistic interaction of AA9 and cellulases during the enzymatic hydrolysis of biomass. *Energ. Environ. Sci.* **7**, 2308–2315 (2014).
19. G. Müller, A. Várnai, K. S. Johansenn, V. G. H. Eijsink, S. J. Horn, Harnessing the potential of LPMO-containing cellulase cocktails poses new demands on processing conditions. *Biotechnol. Biofuels* **8**, 187 (2015).
20. P. Chylenski, Z. Forsberg, J. Ståhlberg, A. Várnai, M. Lersch, O. Bengtsson, S. Sæbø, S. J. Horn, V. G. H. Eijsink, Development of minimal enzyme cocktails for hydrolysis of sulfite-pulped lignocellulosic biomass. *J. Biotechnol.* **246**, 16–23 (2017).
21. K. -E. L. Eriksson, R. A. Blanchette, P. Ander, *Microbial and Enzymatic Degradation of Wood and Wood Components* (Springer-Verlag, 1990).
22. A. V. Wymelenberg, J. Gakell, M. Mozuch, P. Kersten, G. Sabat, D. Martinez, D. Cullen, Transcriptome and secretome analyses of *Phanerochaete chrysosporium* reveal complex patterns of gene expression. *Appl. Environ. Microbiol.* **75**, 4058–4068 (2009).
23. M. Tachioka, A. Nakamura, T. Ishida, K. Igarashi, M. Samejima, Crystal structure of a family 6 cellobiohydrolase from the basidiomycete *Phanerochaete chrysosporium*. *Acta. Crystallogr. F. Struct. Biol. Commun.* **73**, 398–403 (2017).
24. I. G. Muñoz, W. Ubhayasekera, H. Henriksson, I. Szabó, G. Pettersson, G. Johansson, S. L. Mowbray, J. Ståhlberg, Family 7 cellobiohydrolases from *Phanerochaete chrysosporium*: Crystal structure of the catalytic module of Cel7D (CBH58) at 1.32 Å resolution and homology models of the isozymes. *J. Mol. Biol.* **324**, 1097–1111 (2001).
25. A. Nakamura, H. Watanabe, T. Ishida, T. Uchihashi, M. Wada, T. Ando, K. Igarashi, M. Samejima, Trade-off between processivity and hydrolytic velocity of cellobiohydrolases at the surface of crystalline cellulose. *J. Am. Chem. Soc.* **136**, 4584–4592 (2014).
26. M. Wu, G. T. Beckham, A. M. Larsson, T. Ishida, S. Kim, C. M. Payne, M. E. Himmel, M. F. Crowley, S. J. Horn, B. Westereng, K. Igarashi, M. Samejima, J. Ståhlberg, V. G. H. Eijsink, M. Sandgren, Crystal structure and computational characterization of the lytic polysaccharide monooxygenase GH61D from the basidiomycota fungus *Phanerochaete chrysosporium*. *J. Biol. Chem.* **288**, 12828–12839 (2013).
27. B. Westereng, T. Ishida, G. Vaaje-Kolstad, M. Wu, V. G. H. Eijsink, K. Igarashi, M. Samejima, J. Ståhlberg, S. J. Horn, M. Sandgren, The putative endoglucanase *Pc*GH61D from *Phanerochaete chrysosporium* is a metal-dependent oxidative enzyme that cleaves cellulose. *PLoS ONE* **6**, e27807 (2011).
28. M. Wada, L. Heux, J. Sugiyama, Polymorphism of cellulose I family: Reinvestigation of cellulose IV_I. *Biomacromolecules* **5**, 1385–1391 (2004).
29. I. von Ossowski, J. Ståhlberg, A. Koivula, K. Piens, D. Becker, H. Boer, R. Harle, M. Harris, C. Divne, S. Mahdi, Y. Zhao, H. Driguez, M. Claeyssens, M. L. Sinnott, T. T. Teeri, Engineering the exo-loop of *Trichoderma reesei* cellobiohydrolase, Cel7A. A comparison with *Phanerochaete chrysosporium* Cel7D. *J. Mol. Biol.* **333**, 817–829 (2003).
30. G. T. Beckham, J. F. Matthews, B. Peters, Y. J. Bomble, M. E. Himmel, M. F. Crowley, Molecular-level origins of biomass recalcitrance: Decrystallization free energies for four common cellulose polymorphs. *J. Phys. Chem. B* **115**, 4118–4127 (2011).
31. C. M. Payne, M. E. Himmel, M. F. Crowley, G. T. Beckham, Decrystallization of oligosaccharides from the cellulose Iβ surface with molecular simulation. *J. Phys. Chem. Lett.* **2**, 1546–1550 (2011).
32. J. V. Vermaas, M. F. Crowley, G. T. Beckham, C. M. Payne, Effects of lytic polysaccharide monooxygenase oxidation on cellulose structure and binding of oxidized cellulose oligomers to cellulases. *J. Phys. Chem. B* **119**, 6129–6143 (2015).
33. T. Uchiyama, T. Uchihashi, A. Nakamura, H. Watanabe, S. Kaneko, M. Samejima, K. Igarashi, Convergent evolution of processivity in bacterial and fungal cellulases. *Proc. Natl. Acad. Sci. U.S.A.* **117**, 19896–19903 (2020).
34. M. Wada, H. Chanzy, Y. Nishiyama, P. Langan, Cellulose III_I crystal structure and hydrogen bonding by synchrotron x-ray and neutron fiber diffraction. *Macromolecules* **37**, 8548–8555 (2004).
35. K. Igarashi, M. Samejima, K. -E. Eriksson, Cellobiose dehydrogenase enhances *Phanerochaete chrysosporium* cellobiohydrolase I activity by relieving product inhibition. *Eur. J. Biochem.* **253**, 101–106 (1998).
36. S. J. Christensen, J. Kari, S. F. Badino, K. Borch, P. Westh, Rate-limiting step and substrate accessibility of cellobiohydrolase Cel6A from *Trichoderma reesei*. *FEBS J.* **285**, 4482–4493 (2018).
37. K. Igarashi, A. Koivula, M. Wada, S. Kimura, M. Penttilä, M. Samejima, High speed atomic force microscopy visualizes processive movement of *Trichoderma reesei* cellobiohydrolase I on crystalline cellulose. *J. Biol. Chem.* **284**, 36186–36190 (2009).

38. M. Eibinger, J. Sattelkow, T. Ganner, H. Plank, B. Nidetzky, Single-molecule study of oxidative enzymatic deconstruction of cellulose. *Nat. Commun.* **8**, 894 (2017).
39. T. Isaksen, B. Westereng, F. L. Aachmann, J. W. Agger, D. Kracher, R. Kittl, R. Ludwig, D. Haltrich, V. G. H. Eijsink, S. J. Horn, A C4-oxidizing lytic polysaccharide monooxygenase cleaving both cellulose and cello-oligosaccharides. *J. Biol. Chem.* **289**, 2632–2642 (2014).
40. V. V. Vu, W. T. Beeson, C. M. Philips, J. H. D. Cate, M. A. Marletta, Determinants of regioselective hydroxylation in the fungal polysaccharide monooxygenases. *J. Am. Chem. Soc.* **136**, 562–565 (2014).
41. A. Karnaouri, M. N. Muraleedharan, M. Dimarogona, E. Topakas, U. Rova, M. Sandgren, P. Christakopoulos, Recombinant expression of thermostable processive *Mt*EG5 endoglucanase and its synergism with *Mt*LPMO from *Myceliophthora thermophila* during the hydrolysis of lignocellulosic substrates. *Biotechnol. Biofuels* **10**, 126 (2017).
42. P. Limsakul, P. Phitsuwan, R. Waeonukul, P. Pason, C. Tachaapaikoon, K. Poomputsa, A. Kosugi, M. Sakka, K. Sakka, K. Ratanakhanokchai, A novel AA10 from *Paenibacillus curdlanolyticus* and its synergistic action on crystalline and complex polysaccharides. *Appl. Microbiol. Biotechnol.* **104**, 7533–7550 (2020).
43. K. Igarashi, M. Maruyama, A. Nakamura, T. Ishida, M. Wada, M. Samejima, Degradation of crystalline celluloses by *Phanerochaete chrysosporium* cellobiohydrolase II (Cel6A) heterologously expressed in methylotrophic yeast *Pichia pastoris*. *J. Appl. Glycosci.* **59**, 105–110 (2012).
44. M. Yoshida, T. Ohira, K. Igarashi, H. Nagasawa, K. Aida, B. M. Hallberg, C. Divne, T. Nishino, M. Samejima, Production and characterization of recombinant *Phanerochaete chrysosporium* cellobiose dehydrogenase in the methylotrophic yeast *Pichia pastoris*. *Biosci. Biotechnol. Biochem.* **65**, 2050–2057 (2001).
45. K. Igarashi, T. Uchihashi, A. Koivula, M. Wada, S. Kimura, T. Okamoto, M. Penttilä, T. Ando, M. Samejima, Traffic jams reduce hydrolytic efficiency of cellulase on cellulose surface. *Science* **333**, 1279–1282 (2011).
46. K. Igarashi, T. Uchihashi, A. Koivula, M. Wada, S. Kimura, M. Penttilä, T. Ando, M. Samejima, Visualization of cellobiohydrolase I from *Trichoderma reesei* moving on crystalline cellulose using high-speed atomic force microscopy. *Methods Enzymol.* **510**, 169–182 (2012).
47. K. Igarashi, T. Uchihashi, T. Uchiyama, H. Sugimoto, M. Wada, S. Suzuki, S. Sakuda, T. Ando, T. Watanabe, M. Samejima, Two-way traffic of glycoside hydrolase family 18 processive chitinases on crystalline chitin. *Nat. Commun.* **5**, 3975 (2014).
48. G. T. Beckham, M. F. Crowley, Examination of the α-chitin structure and decrystallization thermodynamics at the nanoscale. *J. Phys. Chem. B* **115**, 4516–4522 (2011).
49. J. C. Phillips, R. Braun, W. Wang, J. Gumbart, E. Tajkhorshid, E. Villa, C. Chipot, R. D. Skeel, L. Kalé, K. Schulten, Scalable molecular dynamics with NAMD. *J. Comput. Chem.* **26**, 1781–1802 (2005).
50. O. Guvench, E. R. Hatcher, R. M. Venable, R. W. Pastor, A. D. Mackerell, CHARMM additive all-atom force field for glycosidic linkages between hexopyranoses. *J. Chem. Theory Comput.* **5**, 2353–2370 (2009).
51. W. L. Jorgensen, J. Chandrasekhar, J. D. Madura, R. W. Impey, M. L. Klein, Comparison of simple potential functions for simulating liquid water. *J. Chem. Phys.* **79**, 926–935 (1983).
52. R. Kubo, The fluctuation-dissipation theorem. *Rep. Prog. Phys.* **29**, 255–284 (1966).
53. S. E. Feller, Y. Zhang, R. W. Pastor, B. R. Brooks, Constant pressure molecular dynamics simulation: The Langevin piston method. *J. Chem. Phys.* **103**, 4613–4621 (1995).
54. S. Miyamoto, P. A. Kollman, Settle: An analytical version of the SHAKE and RATTLE algorithm for rigid water models. *J. Comput. Chem.* **13**, 952–962 (1992).
55. U. Essmann, L. Perera, M. L. Berkowitz, T. Darden, H. Lee, L. G. Pedersen, A smooth particle mesh Ewald method. *J. Chem. Phys.* **103**, 8577–8593 (1995).
56. W. Humphrey, A. Dalke, K. Schulten, VMD: Visual molecular dynamics. *J. Mol. Graph.* **14**, 33–38 (1996).
57. C. R. Harris, K. J. Millman, S. J. van der Walt, R. Gommers, P. Virtanen, D. Cournapeau, E. Wieser, J. Taylor, S. Berg, N. J. Smith, R. Kern, M. Picus, S. Hoyer, M. H. van Kerkwijk, M. Brett, A. Haldane, J. F. Del Río, M. Wiebe, P. Peterson, P. Gérard-Marchant, K. Sheppard, T. Reddy, W. Weckesser, H. Abbasi, C. Gohlke, T. E. Oliphant, Array programming with NumPy. *Nature* **585**, 357–362 (2020).
58. J. D. Hunter, Matplotlib: A 2D graphics environment. *Comput. Sci. Eng.* **9**, 90–95 (2007).

Acknowledgments

Funding: This research was supported by Grants-in-Aid for Innovative Areas (nos. 18H05494 to K.I. and 21H00393 and 20H04669 to T.Uchih.) from the Japanese Ministry of Education, Culture, Sports, Science and Technology (MEXT); by Grants-in-Aid for Scientific Research (B: no. 19H03013 to K.I. and C: no. 15 K07383 to T.Uchiy.; B: no. 21H01772 to T.Uchih.) from the Japan Society for the Promotion of Science (JSPS); and by the Environment Research and Technology Development Fund nos. JPMEERF21S11900 and JPMEERF21S11902 (to K.I.) from the Environmental Restoration and Conservation Agency of Japan (ERCA). K.I. thanks the Business Finland for the support of the Finland Distinguished Professor Program "Advanced approaches for enzymatic biomass utilization and modification (BioAD)". This work was authored, in part, by the Alliance for Sustainable Energy LLC, the manager and operator of the National Renewable Energy Laboratory for the U.S. Department of Energy (DOE) under contract no. DE-AC36-08GO28308. J.V.V., M.F.C., and G.T.B. acknowledge funding from the U.S. Department of Energy Office of Energy Efficiency and Renewable Energy Bioenergy Technologies Office. G.T.B. also acknowledges funding from the Center for Bioenergy Innovation, which is a U.S. DOE Bioenergy Research Center supported by the Office of Biological and Environmental Research in the DOE Office of Science. J.V.V. acknowledges current support from the Basic Energy Science office within the DOE Office of Science (DE-FG02-91ER20021). The research was performed using computational resources sponsored by the Department of Energy's Office of Energy Efficiency and Renewable Energy located at the National Renewable Energy Laboratory. **Author contributions:** T.Uchiy. and A.N. conducted the experiments; T.Uchih. made the HS-AFM observations; T.Uchiy. analyzed images; A.N. prepared the crystalline cellulose I_α and enzymes (Cel7D and Cel6A); T.I. and M.S. contributed to cloning and expression of AA9D. J.V.V., M.F.C., and G.T.B. designed and carried out MD simulations of crystalline cellulose; T.Uchiy. and K.I. designed all the experiments and wrote the manuscript. All authors discussed the results and commented on the manuscript. **Competing interests:** The authors declare that they have no competing interests. **Data and materials availability:** All data needed to evaluate the conclusions in the paper are present in the paper and/or the Supplementary Materials.

Submitted 22 August 2022
Accepted 21 November 2022
Published 23 December 2022
10.1126/sciadv.ade5155

ScienceAdvances

Lytic polysaccharide monooxygenase increases cellobiohydrolases activity by promoting decrystallization of cellulose surface

Taku Uchiyama, Takayuki Uchihashi, Takuya Ishida, Akihiko Nakamura, Josh V. Vermaas, Michael F. Crowley, Masahiro Samejima, Gregg T. Beckham, and Kiyohiko Igarashi

Sci. Adv., **8** (51), eade5155.
DOI: 10.1126/sciadv.ade5155

Science Advances (ISSN) is published by the American Association for the Advancement of Science. 1200 New York Avenue NW, Washington, DC 20005. The title *Science Advances* is a registered trademark of AAAS.